IEEE Access
Multidisciplinary | Rapid Review | Open Access Journal

Received February 9, 2021, accepted February 23, 2021, date of publication March 8, 2021, date of current version March 17, 2021.

Digital Object Identifier 10.1109/ACCESS.2021.3064359

A Robust Fuzzy PD Inverse Dynamics Decoupling Control of Spherical Motion Mechanism With Fuzzy Linear Extended State Observer

BIN BIAN AND LIANG WANG
School of Automation Science and Electrical Engineering, Beihang University, Beijing 100191, China
Corresponding author: Liang Wang (wangliang@buaa.edu.cn)

This work was supported by the National Natural Science Foundation of China under Grant 50575014.

ABSTRACT In this paper, a robust adaptive fuzzy proportional-derivative inverse dynamics decoupling control scheme with fuzzy-based linear extended state observer (FLESO) is presented and applied to the trajectory tracking control of a two degree-of-freedom (2-DOF) spherical motion mechanism (SMM). The dynamics of the SMM has the characteristics of multivariable nonlinearity, uncertainties and strong coupling. Uncertainties like the modeling errors and external disturbances affect the tracking performance, and coupling increases the difficulty of controller design and reduces the tracking precision. Therefore, a novel hybrid control scheme that is composed of a fuzzy proportional-derivative (FPD) feedback control with varying gains, inverse dynamic model-based feed-forward decoupling term, FLESO with varying bandwidth, and robust term is developed. The novel control strategy combines the advantages of simplicity and easy design of the FPD control, the effectiveness of the FLESO to handle the modeling errors and external disturbances, and the robustness of the robust term to estimation errors of the FLESO. First, introduce the structure of the SMM and establish the dynamic model. Second, the feed-forward decoupling principle is derived based on the inverse dynamic model. Then the FPD control with two-inputs and two-outputs is designed, whose rule base is derived by the phase plane method. The linear extended state observer is designed, whose bandwidth is tuned via the fuzzy logic system. Furthermore, the asymptotic stability of the proposed controller is proved by the Lyapunov theorem. Finally, the high tracking performance of the proposed controller is validated via both simulation and experiment results.

INDEX TERMS Robust and adaptive control, fuzzy proportional-derivative control, fuzzy-based linear extended state observer, inverse dynamics decoupling control, spherical motion mechanism.

I. INTRODUCTION

Multi-DOF spherical motion generation devices, which are generally composed of at least two rotary motors and some intermediate connecting parts in serial or parallel form, have been widely applied in industry such as robotic joints and orienting devices [1]–[3]. For accomplishing spherical motion, the above mentioned mechanisms frequently have bulky structures and complex motions. To achieve a compact design, one of methods is designing an integrated actuator without the intermediate transmission mechanisms to generate multi-DOF motion. In this paper, we investigate a novel 2-DOF hydraulic spherical motion mechanism (SMM) which can accomplish a 2-DOF smooth spherical motion in a single joint [4]. It has the advantages of a compact structure, low inertia and high stiffness. However, since the mentioned SMM has the features of multivariable nonlinearity, uncertainties and strong coupling, the conventional linear controllers can no longer satisfy the tracking control requirements in terms of high tracking precision and robustness and so forth. Therefore, it is essential to develop an effective and efficient tracking control strategy for achieving satisfactory control performance. So far, there have been plenty of advanced control strategies to settle the control problems caused by nonlinearity, uncertainties and strong coupling, such as fuzzy logic control [5], [6], neural network control [7], [8] and sliding mode control [9] and so forth. These studies show that the aforementioned controllers can provide high control performance against nonlinearity and uncertainties. Nevertheless, the traditional neural networks

The associate editor coordinating the review of this manuscript and approving it for publication was Okyay Kaynak.

demand extensive representative training sample and amount of online computation time. The chattering phenomenon of sliding mode control might result in the system instability. These drawbacks limit their applications for the real time control.

These motivate us to develop an efficient control strategy for the SMM to compensate for the model uncertainties and external disturbances, which can not only provide the satisfactory control performance, but also has the simple structure and low computation. Fuzzy control introduced in [10], [11] as a primary model-free control approach, which utilizes human linguistic to describe the nonlinear mapping relationship of inputs and outputs based on fuzzy set theory, has the outstanding capability to cope with the nonlinearities and uncertainties [12]. On the other hand, although the traditional PID controller does not handle nonlinearities and uncertainties effectively, it has the virtues of a simple structure, easy for hardware implementation and low cost [13]. Therefore, a better controller by combining the fuzzy with PID was studied [5], [14]. Liu *et al*. [15] applied the fuzzy PID controller in the field of nuclear to control reactor power. Jin *et al*. [16] utilized the fuzzy PID controller to enhance the output precision of the transplanting manipulator for hydraulic seeding picking-up mechanism in the presence of nonlinearity and external factors. Pan *et al*. [17] designed a fuzzy PID controller for an exoskeleton-human robot system and verified the performance via co-simulations. The above mentioned literatures show that fuzzy PID controllers have not only the relatively simple structure but also the favorable control performance.

The inverse dynamic model-based feed-forward control with the simple structure is widely employed to linearize and decouple the nonlinear coupled systems [18], [19]. However, it requires a precision dynamic model and has no capability to handle the model uncertainties and external disturbances. To weaken the influence of model uncertainties and external disturbances, several disturbance observers have been studied to estimate and compensate for them, such as disturbance estimator [20], [21], nonlinear disturbance observer [22] and extended state observer [23], [24] and so forth. The linear extended state observer regards all factors impacting the motion of plant in terms of the model uncertainties and external disturbances as the total disturbances to estimate. Compared with the other disturbance observers, it has the advantages of a simple structure, less demand of the plant dynamics and higher estimation precision [25]. Therefore, the linear extended state observer is selected as a disturbance observer for the SMM.

In this paper, a novel hybrid robust adaptive control scheme named FPDESO that consists of a FPD feedback control with varying gains, inverse dynamic model-based feed-forward decoupling term, FLESO with varying bandwidth, tracking differentiator (TD) and robust term is proposed. The PD feedback control whose P- and D-gains are regulated via the fuzzy system is used to speed up the convergence rate. The fuzzy rule bases are designed by the phase plane method.

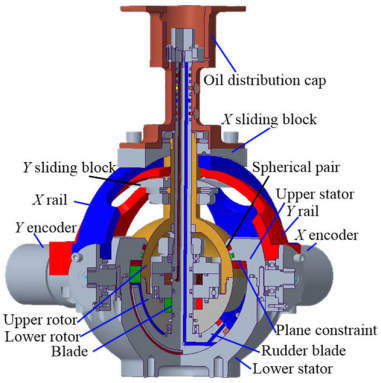

FIGURE 1. Computer-aided design model of the SMM.

The FLESO is utilized to estimate the model uncertainties and external disturbances, and then the corresponding compensation is exerted to suppress the influence of them to improve the decoupling accuracy and robustness of the controller. Moreover, the bandwidth of the linear extended state observer (LESO) is tuned via the fuzzy system to improve estimation precision. To further enhance the robustness, a robust term is increased to amend estimation errors of the FLESO. The TD is employed to filter sensor noise. The proposed control law combines the merits of the simple structure of the FPD control, the effectiveness of the FLESO to handle the model uncertainties and disturbances, and the robustness of the robust term to the estimation errors.

The rest sections of this paper are arranged as follows. Section II establishes the dynamic model of the SMM. Then the hybrid controller composed of the FPD feedback control along with the inverse dynamic model-based feed-forward decoupling term, TD, FLESO, and robust term is designed in Section III. Section IV proves the asymptotic stability of the proposed controller. Section V illustrates the simulation and experimental results. Finally, some conclusions are drawn in Section VI.

II. ARCHITECTURE AND DYNAMICS MODELING

A. ARCHITECTURE

As shown in Fig. 1, the computer-aided design (CAD) model of the SMM is presented. It is composed of two rotors (upper and lower rotors), two stators (upper and lower stators), a rudder blade, a measurement system (X and Y rails, X and Y sliding blocks, and X and Y encoders), and hydraulic actuators (swing and spin hydraulic motors).

Since the swing and spin motors are integrated into one rotor, a single rotor can accomplish two degrees of freedom motion: one is tilting around the X_0 axis, and the other is spinning around the Z_0 axis, which are actuated by the swing and spin hydraulic motors respectively, as depicted in Fig. 2. The detailed operation principle has been described in [4].

B. DYNAMICS MODELING

The orientation of the SMM is represented by a coordinate transformation of the tilt–torsion–spin $(\beta, -\alpha, \theta)$ of the rotor,

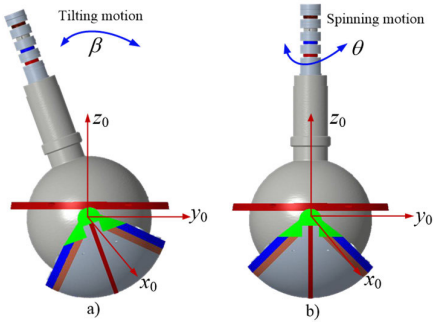

FIGURE 2. Motions of the SMM a) Tilting motion b) Spinning motion.

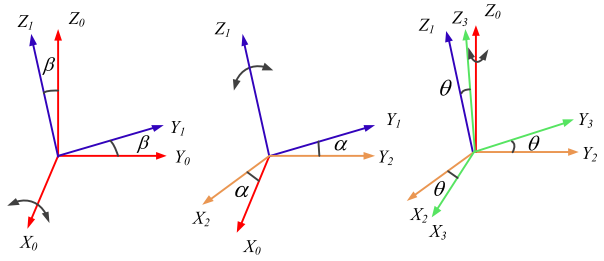

FIGURE 3. Coordinate transformation of tilt–torsion–spin.

as illustrated in Fig. 3. The rotation matrix determining the orientation of the SMM based on the $X_0Z_1Z_0$ conversions can be written as

$$R_{X_0Z_1Z_0} = \begin{bmatrix} c\alpha c\theta + s\alpha c\beta s\theta & s\alpha c\theta - c\alpha c\beta s\theta & s\beta s\theta \\ c\alpha s\theta - s\alpha c\beta c\theta & s\alpha s\theta + c\alpha c\beta c\theta & -s\beta c\theta \\ -s\alpha s\beta & c\alpha s\beta & c\beta \end{bmatrix} \tag{1}$$

where c and s denote "cosine" and "sine", respectively. The dynamic model of the SMM in the generalized coordinates $q = [\alpha \ \beta]^T$ can be formulated by the Lagrange's equation, as follows:

$$M(q)\ddot{q} + C(q, \dot{q})\dot{q} + G(q) + F(\dot{q}) + \xi_{edis} = \tau_c \tag{2}$$

where $M(q)$ denotes the inertial matrix, $C(q, \dot{q})$ is the Coriolis and centripetal term which can be ignored in low-speed motion, $G(q)$ is the gravitational term, $F(\dot{q})$ is the vector of the viscous friction, τ_c is the control torque vector in the generalized coordinate system and ξ_{edis} denotes the external disturbances including load fluctuation and impact of the external environment, the detailed expressions of $M(q)$, $C(q, \dot{q})$ and $G(q)$ are given in the Appendix A.

III. CONTROLLER DESIGN

A. MODEL-BASED FEED-FORWARD DECOUPLING

It can be seen in (2) that the dynamics of the SMM has a nonlinear characteristic as many interactive coupling terms exist in the dynamic model. In this section, based on the inverse dynamic model and the estimation of uncertainties, the coupled system is transformed into an integral series system through feed-forward compensation to achieve the purpose of approximate decoupling. Meanwhile, note that modeling errors cannot be avoided in the process of dynamics modeling. Considering the effects of model uncertainties, (2) can be rewritten as

$$\hat{M}(q)\ddot{q} + \hat{C}(q, \dot{q})\dot{q} + \hat{G}(q) + F(\dot{q}) + \xi_{edis} = \tau_c \tag{3}$$

where $\hat{M}(q) = M(q) + \Delta M(q)$ is the actual inertial matrix, $\hat{C}(q, \dot{q}) = C(q, \dot{q}) + \Delta C(q, \dot{q})$ is the actual Coriolis and centripetal term, $\hat{G}(q) = G(q) + \Delta G(q)$ is the actual gravitational term, and $\Delta M(q)$, $\Delta C(q, \dot{q})$ and $\Delta G(q)$ represent the modeling errors.

Let

$$\xi_{idis} = \Delta M(q)\ddot{q} + \Delta C(q, \dot{q})\dot{q} + \Delta G(q) + F(\dot{q}) \tag{4}$$

where ξ_{idis} is the internal disturbances containing parameter variations and modeling errors. Then, (3) can be rewritten as

$$M(q)\ddot{q} + C(q, \dot{q})\dot{q} + G(q) + \xi_{dis} = \tau_c \tag{5}$$

where $\xi_{dis} = \xi_{idis} + \xi_{edis}$ denotes the total disturbances.

The candidate feed-forward compensation term is designed as

$$\tau_c = M(q)u + C(q, \dot{q})\dot{q} + G(q) \tag{6}$$

where u is the control law.

Substituting (6) into (5), (5) can then be rewritten as

$$M(q)\ddot{q} + \xi_{dis} = M(q)u \tag{7}$$

If the total disturbances containing the internal and external disturbances can be estimated, and then compensated for, (6) can be redesigned as

$$\tau_c = M(q)u + C(q, \dot{q})\dot{q} + G(q) + \tilde{\xi}_{dis} \tag{8}$$

where $\tilde{\xi}_{dis}$ denotes the estimate value of the total disturbances. If the disturbance observer has enough high precision, that is, $\tilde{\xi}_{dis} \approx \xi_{dis}$, the influence of the total disturbances can be eliminated.

Substituting (8) into (5), (5) can be modified as

$$M(q)\ddot{q} = M(q)u \tag{9}$$

Since $M(q)$ is a symmetric positive definite matrix, the following equation can be obtained

$$\ddot{q} = u \tag{10}$$

Consequently, the coupled SMM can be decoupled. And the higher the estimate accuracy of the disturbance observer is, the better the decoupling performance is.

B. FUZZY PD CONTROL

The traditional linear PD controller has been widely used in the industrial field because of its simple structure, easy hardware implementation, and wide applicability and so forth. The linear PD control law can be given as

$$u = K_p(e)e(t) + K_d(e)\dot{e}(t) \tag{11}$$

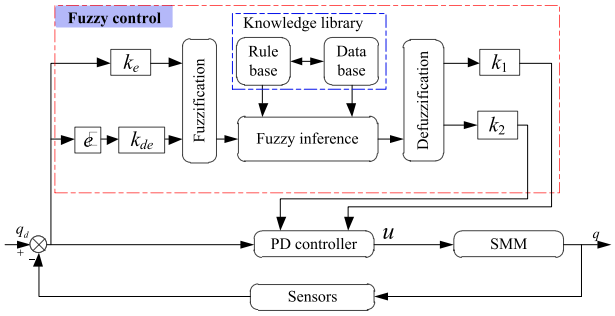

FIGURE 4. Fuzzy PD control.

where $K_p(e) \in \Re^{2\times 2}$, $K_d(e) \in \Re^{2\times 2}$ are the proportional and derivative gains. $e(t) = q_d(t) - q(t)$ and $\dot{e}(t) = \dot{q}_d(t) - \dot{q}(t)$ are the tracking error and change of error, respectively. $q_d(t)$ and $q(t)$ are the desired and actual trajectories, respectively.

Nevertheless, the performance of linear PD controller is not ideal for systems with nonlinearity, model uncertainties and external disturbances. And the gains of linear PD controller are mainly adjusted manually. As a knowledge-based control approach, fuzzy controller that uses the experience of expert to establish control rules and realize automatic control is particularly suitable for complex system with nonlinearity and uncertainties. Therefore, to enhance the tracking performance, this paper utilizes a two-dimensional fuzzy controller to tune the parameters of the PD controller in the real time. The fuzzy controller is composed of the fuzzification, rule base, fuzzy reasoning and defuzzification, as illustrated in Fig. 4. The self-adjusting proportional and derivative gains of the PD controller can be given as

$$\begin{cases} k_{pj}(e) = k_{pj_0} + k_1 f_k^j(k_e) \\ k_{dj}(\dot{e}) = k_{dj_0} + k_2 f_k^j(k_{de}) \end{cases} \quad j = \alpha, \beta \qquad (12)$$

where k_1 and k_2 are the scaling coefficients of fuzzy output, respectively. $f_k^j(\cdot)$ represents the fuzzy operation with respect to j at time k. k_{pj_0}, k_{dj_0} are the initial values of the proportional and derivative gains, respectively.

The detailed design process of the fuzzy system is explained as follows:

Step 1: Fuzzification

Here, the tracking error e and change of error $\dot{e}(ce)$ are utilized as the input variables and the correction factors of PD are selected as the output variables, i.e., $f_k(k_e)$ and $f_k(k_{de})$, whose universes of discourse (UOD) are all normalized to the domain of $[-1, 1]$. The linguistic labels corresponding to the UOD of inputs and outputs are divided into Negative big (NB), Negative medium (NM), Negative small (NS), Zero (ZE), Positive small (PS), Positive medium (PM) and Positive big (PB).

Since the triangular type of membership functions (MFs) has the merits of simplicity and high computation efficiency, it is selected to distribute the fuzzy sets equally for the input variables [26], as illustrated in Fig. 5(a). Analogously, the Gaussian type of MFs with the features of smooth and non-zero at all points, which is more suitable to describe complicated fuzzy relationship, is utilized for the fuzziness of output variables, as depicted in Fig. 5(b). An intersection level of 0.5 and an intersection ratio of 1 between two adjacent MFs are employed, because it can provide faster rise time, less settling time and smaller overshot, as pointed out in [27].

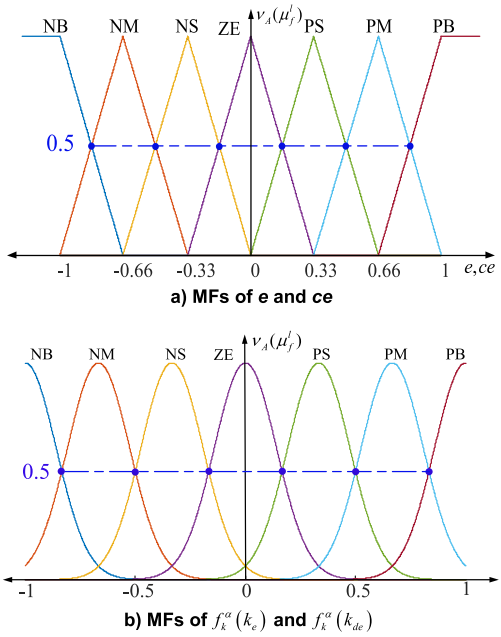

FIGURE 5. MFs of input and output variables.

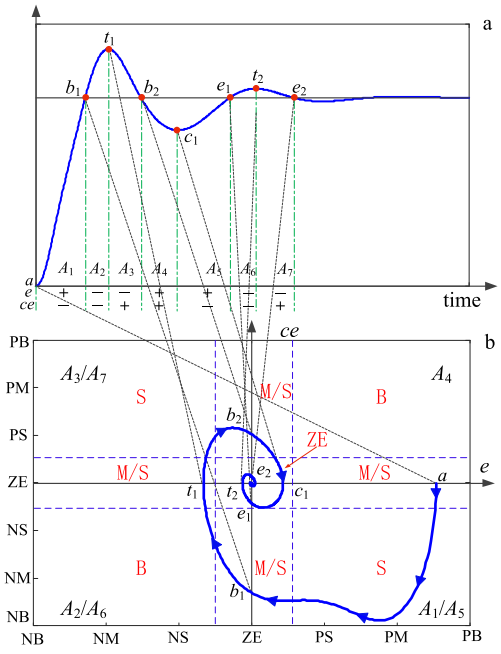

FIGURE 6. Rule analysis for α a) Step response b) (e, ce) state space.

Step 2: Rule base

As the most important part of the fuzzy controller, the rule base reflects the operation process. Generally, the rule base is extracted from the practical experience of the skilled

operators, which makes rules design more subjective, difficult and less universal. One of methods to design rules is mapping from the step response in time domain to the phase plane of (e, ce),named the phase plane method. This method combines the knowledge of step response with the phase plane trajectory to assess the control rules. The step response can provide the information of error e and change of error ce. Furthermore, the time domain dynamic features of the system in terms of overshoot, rise time and settling time are essential for the corresponding phase plane trajectory analysis.

Since different stages have different performances, the step response in time domain can be divide into seven regions ($A_1 - A_7$), four intersection points (b_1, b_2, e_1, e_2) and three peak valley points (t_1, t_2, c_1). And the sign of e and ce changes in the different regions, as shown in Fig. 6(a). The phase plane of (e, ce) is established based on the above step response, which is divided into four quadrants corresponding to the seven areas of the step response ($A_1 - A_7$). Moreover, the linguistic labels are considered as the coordinates of the phase plane, as depicted in Fig. 6(b). And then formulate the rules based on the characteristics of e and ce in different areas [28], as follows:

The output is approaching nearer toward the set point in regions A_1, A_3 and A_5, the small or medium gain is adopted to avoid overshoot or undershoot and reduce the settling time. In regions A_2, A_4 and A_6, the output is moving upward or downward farther away from the command, the big gain is considered to reduce the further deterioration of the situation. Moreover, when the state is close to the steady state, which means that the output has just arrived or left the set point but is moving away upward or downward from the set point rapidly. In this condition, consider the medium gain to eliminate overshoot or undershoot.

Criterion 1: The sign of rules

- If $e = 0$ and $ce = 0$, consider
$$f_k^j(k_e) = f_{k-1}^j(k_e) \text{ and } f_k^j(k_{de}) = f_{k-1}^j(k_{de}).$$
- If $e = 0$, i.e., b_1, b_2, e_1 and e_2, consider
$$\text{sign}\left(f_k^j(k_{de})\right) = \text{sign}(ce).$$
- If $ce = 0$, i.e., t_1, c_1 and t_2, consider
$$\text{sign}\left(f_k^j(k_e)\right) = \text{sign}(e).$$
- If e will approach zero at a satisfactory rate, consider
$$f_k^j(k_e) = f_{k-1}^j(k_e) \text{ and } f_k^j(k_{de}) = f_{k-1}^j(k_{de}).$$
- In areas $A_1/A_2/A_5/A_6$, $ce < 0$, consider $f_k^j(k_e), f_k^j(k_{de}) > 0$.
- In areas $A_3/A_4/A_7$, $ce > 0$, consider $f_k^j(k_e), f_k^j(k_{de}) < 0$.
- Rules for three segments, b_1t_1, e_1t_2 and b_2c_1 should prevent the overshoot in A_2/A_6 or undershoot in A_4.
- Rules for four segments, ab_1, t_1b_2, c_1e_1 and t_2e_2 should speed up the response in $A_1/A_3/A_5/A_7$.
- In the equilibrium points, consider $f_k^j(k_e), f_k^j(k_{de}) = 0$.

Criterion 2: The magnitude of rules

1) At peak points, t_1, t_2 and valley point, c_1, rule for the self-adjusting proportional gain is as follows:
$$f_k^j(k_e) = \frac{1 - k_{pj_0}}{k_1}, \quad ce = 0 \tag{13}$$
2) In cross-over areas, to decrease overshoot or undershoot in areas $A_2/A_4/A_6$, consider rules as follows:
$$\begin{cases} f_k^j(k_e) = \text{PS or PM}, \ f_k^j(k_{de}) = \text{PS or PM}, & ce > 0 \\ f_k^j(k_e) = \text{NS or NM}, \ f_k^j(k_{de}) = \text{NS or NM}, & ce < 0 \end{cases} \tag{14}$$
3) Rules for areas A_1/A_5 and A_3/A_7 are as follows:
$$\begin{cases} f_k^j(k_e) = \min\left\{(f_0^j(k_e) + \frac{e}{k_1}), \text{PS}\right\} \\ f_k^j(k_{de}) = \min\left\{(f_0^j(k_{de}) + \frac{ce}{k_2}), \text{PS}\right\} \end{cases} \tag{15}$$
In areas A_1 and A_5, rules should be positive.
$$\begin{cases} f_k^j(k_e) = \max\left\{(f_0^j(k_e) + \frac{e}{k_1}), \text{NS}\right\} \\ f_k^j(k_{de}) = \max\left\{(f_0^j(k_{de}) + \frac{ce}{k_2}), \text{NS}\right\} \end{cases} \tag{16}$$
In areas A_3 and A_7, rules should be negative.

Consequently, based on the phase plane trajectory and the behavior of step response, the rule bases for updating gains factors $f_k^\alpha(k_e)$ and $f_k^\alpha(k_{de})$ are listed in Table 1. The designed rule bases have the properties of completeness, consistence, and continuity [29], which can guarantee the targeted fine control in the whole trajectory tracking process.

To obtain good performance, at least one rule is activated in the control process to adapt the current operating condition. For instance, at the time instant t_1, where $e(t_1) = 0.51$ and $ce(t_1) = 0.20$, two MFs were involved, which were PS and PM for error, and ZE and PS for change of error, as shown in Fig. 7. Therefore, there existed four active rules at the time instant t_1 in the process of fuzzy inference. According to the rule bases listed in Table 1, the relevant rules at the time instant t_1 can be given, respectively, as

- $\mathbf{R}^1$: If e = PS and ce = ZE, then $f_k^\alpha(k_e)$ = PM and $f_k^\alpha(k_{de})$ = NS.
- $\mathbf{R}^2$: If e = PS and ce = PS, then $f_k^\alpha(k_e)$ = NM and $f_k^\alpha(k_{de})$ = NS.
- $\mathbf{R}^3$: If e = PM and ce = ZE, then $f_k^\alpha(k_e)$ = PM and $f_k^\alpha(k_{de})$ = NS.
- $\mathbf{R}^4$: If e = PM and ce = PS, then $f_k^\alpha(k_e)$ = NM and $f_k^\alpha(k_{de})$ = NS.

Furthermore, quantify the fuzzy logical "and" for all active rules by means of the Mamdani inference method. And then aggregate the outputs of all active rules to deduce the overall value of fuzzy output at the time instant t_1.

Analogously, the step response and corresponding phase plane trajectory of β are shown in Fig. 26(a)-(b), respectively. And the derived fuzzy rule bases of β for updating gains are listed in Table 7 in the Appendix B.

Step 3: Defuzzification

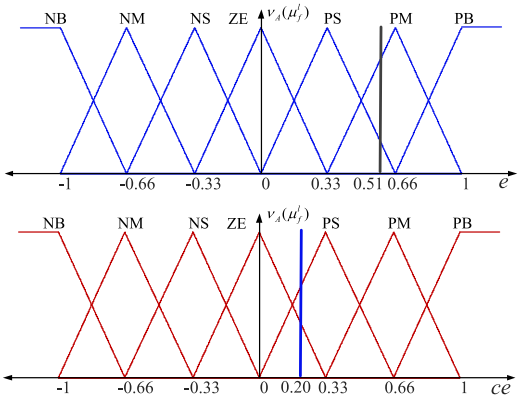

FIGURE 7. MFs of e and ce at the time instant t_1.

TABLE 1. Rules for f_k^{α} (k_e) and f_k^{α} (k_{de}).

ce \ e	NB	NM	NS	ZE	PS	PM	PB
NB	PB\PB	PB\PB	PB\PB	NM\NM	PS\PS	PS\PS	ZE\ZE
NM	PB\PB	PB\PB	PB\PB	NS\NM	PS\PS	ZE\ZE	PS\PS
NS	PB\PM	PB\PM	PM\PM	NS\NM	ZE\ZE	PS\PS	PM\PS
ZE	NM\ZE	NM\NS	NM\NS	ZE\ZE	PM\NS	PM\NS	PM\ZE
PS	NM\NS	NS\NS	ZE\ZE	PS\PM	NM\NS	NM\NS	NM\NS
PM	NS\NS	ZE\ZE	NS\NS	PS\PM	NM\NB	NB\NB	NB\NB
PB	ZE\ZE	NS\NS	NM\NM	PM\PM	NB\NB	NB\NB	NB\NB

A2/A6 B A1/A5 S A3/A7 S A4 B

Defuzzification converts the fuzzy sets to the crisp outputs which act on the plant. The center of gravity defuzzification approach is employed because of its steady and monotonicity. The crisp output value can be written as

$$u_{crisp} = \frac{\int_{\chi} \nu_A(u_f^l) u_f^l du_f^l}{\int_{\chi} \nu_A(u_f^l) du_f^l} \tag{17}$$

where χ and A denote the UOD and fuzzy set of output variables, respectively, u_f^l represents the l-th element in the UOD of the output variables, $\nu_A(u_f^l)$ is the degree of membership with respect to u_f^l.

C. FUZZY-BASED LINEAR EXTENDED STATE OBSERVER

According to the above analysis, to improve the decoupling precision and robustness of the controller, it is significant to design a high-precision disturbance observer to estimate and compensate for the model uncertainties and external disturbances.

Consider the n^{th} nonlinear system as follows:

$$y^{(n)} = g(\dot{y}, \ddot{y}, \cdots, y^{(n-1)}) + f(\dot{y}, \ddot{y}, \cdots, y^{(n-1)}, u, \xi_{edis}) + bu \tag{18}$$

where $g(\cdot)$ is the known system dynamics, $f(\cdot)$ denotes the total disturbances containing the modeling errors and external disturbances, b is a constant value, u is the system input, y is the system output and n denotes the system order.

In this paper, $n = 2$ and $x = [q \ \dot{q}]^T$, (18) can be expressed as

$$\dot{x}_2 = -M^{-1}(x_1)(C(x_1, x_2)x_2 + G(x_1) + \xi_{dis}) + M^{-1}(x_1)u \tag{19}$$

Consider $f(\cdot)$ as an extended state of (19), the state space form of (19) can be expressed as

$$\begin{cases} \dot{x}_1 = x_2 \\ \dot{x}_2 = x_3 - M^{-1}(x_1)(C(x_1, x_2)x_2 \\ \qquad + G(x_1)) + M^{-1}(x_1)u \\ \dot{x}_3 = h(\cdot) \\ y = x_1 \end{cases} \tag{20}$$

where $x_3 = f(\cdot) = -M^{-1}(x_1)\xi_{dis}$ and $h(\cdot) = df(\cdot)/dt$.

Compared with the nonlinear extended state observer (NESO), LESO is more convenient to design and simpler to tune parameters. Consequently, the LESO [30] is applied to the control system of the SMM, which can be designed as

$$\begin{cases} \varepsilon = x_1 - \hat{x}_1 \\ \dot{\hat{x}}_1 = \hat{x}_2 + l_1\varepsilon \\ \dot{\hat{x}}_2 = \hat{x}_3 - M^{-1}(\hat{x}_1)(C(\hat{x}_1, \hat{x}_2)\hat{x}_2 + G(\hat{x}_1)) \\ \qquad + M^{-1}(\hat{x}_1)u + l_2\varepsilon \\ \dot{\hat{x}}_3 = l_3\varepsilon \end{cases} \tag{21}$$

where $\hat{x}_1$, $\hat{x}_2$, and $\hat{x}_3$ are the observed states, l_i, $i = 1, 2, 3$ are the observer gains to be designed.

To simplify parameters tuning, the pole placement method is adopted to make the observer bandwidth the only tuning parameter [31], which can be expressed as

$$(s + \omega_o)^{n+1} = s^{n+1} + l_1 s^n + \cdots + l_n s + l_{n+1} \tag{22}$$

where ω_o denotes the observer bandwidth.

Thus

$$l_1 = 3\omega_o, \quad l_2 = 3\omega_o^2, \quad l_3 = \omega_o^3 \tag{23}$$

The ESO is a high gain observer, which may result in a peaking phenomenon [32]. The fuzzy logic system, which has the advantages of a simple structure and excellent global approximation property, can provide a reasonable trade-off between the convergence rate and the control performance. In this paper, it is utilized to tune the bandwidth of LESO to improve the performance of LESO and achieve the same high precision estimation as NESO [33], as shown in Fig 8.

In order to reduce the number of fuzzy rules and enhance the computational efficiency, the linear combination of the estimation error E and its change $\dot{E}$, $k_{s1}E + k_{s2}\dot{E}$ is applied as the input, and the tuning factor of observer bandwidth f (ω_o) is utilized as the output [34]. The linguistic labels for input are divided into NB, NS, ZE, PS, and PB in the range of $[-1, 1]$. The MFs of input adopt the Gaussian shape, as shown in Fig. 9. Three variable labels for output are designed in the range of [-1, 1], named Big (B), Medium (M), and Small (S), and select the Gaussian shape as the MFs.

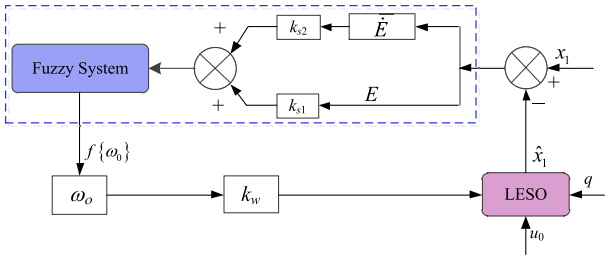

FIGURE 8. FLESO.

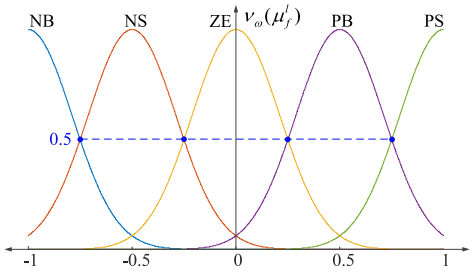

FIGURE 9. MFs of input variable for observer bandwidth tuning.

The following fuzzy rules will be employed to tune the observer bandwidth [34].

- $\mathbf{R}_w^1$: If $k_{s1}E + k_{s2}\dot{E} = \text{NB}$, then $f(\omega) = S$.
- $\mathbf{R}_w^2$: If $k_{s1}E + k_{s2}\dot{E} = \text{NS}$, then $f(\omega) = M$.
- $\mathbf{R}_w^3$: If $k_{s1}E + k_{s2}\dot{E} = \text{ZE}$, then $f(\omega) = L$.
- $\mathbf{R}_w^4$: If $k_{s1}E + k_{s2}\dot{E} = \text{PS}$, then $f(\omega) = M$.
- $\mathbf{R}_w^5$: If $k_{s1}E + k_{s2}\dot{E} = \text{PB}$, then $f(\omega) = S$.

Finally, the center of gravity defuzzification approach is utilized to calculate the crisp output value of the fuzzy logic system, referring to (17).

D. TRACKING DIFFERENTIATOR

Since sensor noise easily distorts the signal and then affects the tracking performance, in order to extract the actual signal reasonably from the measurement signal with random noise, the tracking differentiator is utilized, as following:

The discrete form of TD [35] can be written as

$$\begin{cases} x_1(k+1) = x_1(k) + t \cdot x_2(k) \\ x_2(k+1) = x_2(k) + t \cdot fst(x_1(k) - v(k), x_2(k), \sigma, h) \end{cases} \tag{24}$$

The fast tracking control method is adopted to achieve the tracking and differential of signal as real as possible, the synthesis function of which can be expressed as

$$\begin{cases} fst(x_1(k) - v(k), x_2(k), \sigma, t) = -\sigma \cdot sat(g(k), \sigma) \\ e(k) = x_1(k) - v(k) \\ \delta = h \cdot \sigma, \delta_1 = h \cdot \delta \\ y(k) = e(k) + t \cdot x_2(k) \\ g(k) = \begin{cases} x_2(k) + y(k)/h & |y(k)| < \delta_1 \\ x_2(k) + \frac{sign(y(k)) \cdot \sqrt{8\sigma \cdot |y(k)| + \delta^2} - \delta}{2} & |y(k)| \geq \delta_1 \end{cases} \\ sat(g(k), \delta) = \begin{cases} g(k)/\delta & |g(k)| < \delta \\ sign(g(k)) & |g(k)| \geq \delta \end{cases} \end{cases} \tag{25}$$

where $v(k)$ is the input signal, $x_1(k)$ is the tracking signal with respect to $v(k)$, $x_2(k)$ is the differential of $x_1(k)$, t is the integral step size, δ is the parameter that determines the tracking speed, and h is the filter coefficient, generally, $h > t$.

Based on the aforementioned analysis, this paper proposed a robust and adaptive controller, which is composed of a fuzzy PD feedback control, inverse dynamic model-based feed-forward decoupling term, TD, FLESO and robust term, as shown in Fig. 10.

The proposed control scheme can be expressed as

$$\tau_c = M(q)(\ddot{q}_d + u) + C(q, \dot{q})\dot{q} + G(q) + \tilde{\xi}_{dis} - v \tag{26}$$

where v is the robust term to compensate for the estimation error, $\Delta\xi_{dis} = \xi_{dis} - \tilde{\xi}_{dis}$ is the estimation error, $\|\Delta\xi_{dis}\| \leq b_d$.

with

$$v = -b_d \ \text{sgn}(\dot{e}^T M^{-1}(q)) \tag{27}$$

The first item is the feed-forward compensation term that uses the inverse dynamic model along with the desired acceleration and the actual position and velocity of the end-effector to approximate joint torque. This term that helps to simplify the design of controller can make the nonlinear coupled system achieve approximate linearization and decoupling. It can be expressed as

$$\tau_{c1} = M(q)\ddot{q}_d + C(q, \dot{q})\dot{q} + G(q) \tag{28}$$

The second item as the core part of controller, which is employed to eliminate the tracking error based on the position error, can be expressed as

$$\tau_{c2} = M(q)u \tag{29}$$

The third item is the compensation term of modeling errors and external disturbances, which can be expressed as

$$\tau_{c3} = \tilde{\xi}_{dis} - v \tag{30}$$

To a large extent, the robustness of the control system is directly determined by the suppression effect of the control law on the modeling errors and external disturbances. Therefore, in this paper, one of the most important tasks is to design a disturbance observer with high estimation accuracy.

IV. STABILITY ANALYSIS

The stability of the proposed controller is demonstrated by the Lyapunov direct method. The Lyapunov function candidate is selected as

$$L(e, \dot{e}) = \frac{1}{2}\dot{e}^T\dot{e} + \int_0^e \varphi^T K_p(\varphi)d\varphi \tag{31}$$

where $K_p(e)$ is a positive definite matrix [19].

$$\int_0^e \varphi^T K_p(\varphi)d\varphi = \int_0^{e_1} \varphi_1^T k_{p1}(\varphi_1)d\varphi_1 + \int_0^{e_2} \varphi_2^T k_{p2}(\varphi_2)d\varphi_2$$

Obviously, the first term of $L(e, \dot{e})$ is non-negative. As a Lyapunov function candidate, the second term of $L(e, \dot{e})$ must be a positive definite function, which will be proved in the following.

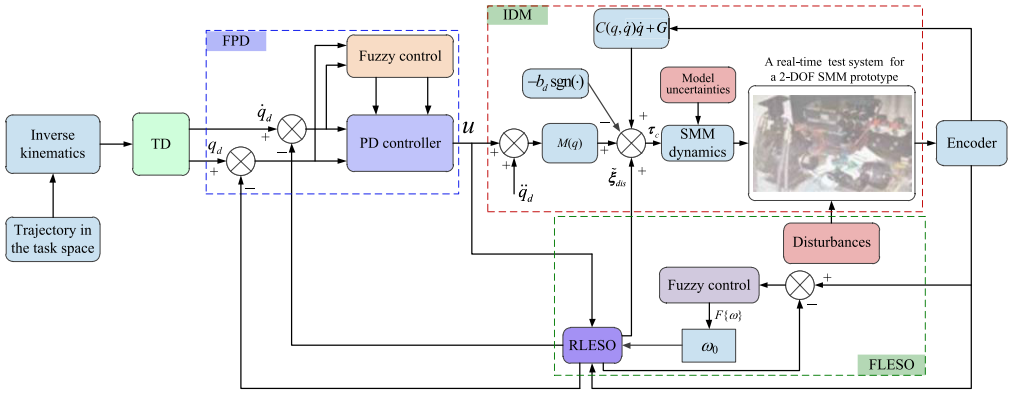

FIGURE 10. Schematic diagram of the proposed FPDESO controller.

Lemma. [36] Consider the diagonal matrix $K_p : \Re^2 \to \Re^{2\times 2}$

$$K_p(e) = \begin{bmatrix} k_{p1}(e_1) & 0 \\ 0 & k_{p2}(e_2) \end{bmatrix}$$

Assume that there exist class K function $\vartheta_i(\cdot)$ such that

$$|x|\, k_{pi}(x) \geq \vartheta_i(|x|), \quad x \in \Re, \quad i = 1, 2$$

Then

$$\int_0^{e_i} |\varphi_i|^T k_{pi}(\varphi_i) d\varphi_i > 0, \quad \forall e_i \neq 0 \in \Re,$$

and

$\int_0^e |\varphi|^T K_p(\varphi) d\varphi \to \infty$ as $|e| \to \infty$.

From (12), note that $|e_j|\, k_{pj}(e_j) \geq \vartheta_j(|e_j|), \quad e_j \in \Re, \ j = 1, 2$. Thus the second term of $L(e, \dot{e})$ is a radially unbounded positive definite function. Hence, $L(e, \dot{e})$ is a positive definite function, i.e., $L(e, \dot{e}) > 0$.

Differentiating (31) with respect to time obtains (32)

$$\begin{aligned} \dot{L}(e, \dot{e}) &= \dot{e}^T \ddot{e} + \frac{d}{dt}\left[\int_0^e \varphi K_p(\varphi)\, d\varphi\right] \\ &= \dot{e}^T \ddot{e} + \sum_{j=1}^{2} \frac{\partial}{\partial e_j}\left[\int_0^{e_j} \varphi_j k_{pj}(\varphi_j)\, d\varphi_j\right] \dot{e}_j \\ &= \dot{e}^T \ddot{e} + \sum_{j=1}^{2} e_j k_{pj}(e_j) \dot{e}_j \\ &= \dot{e}^T \ddot{e} + e^T K_p(e) \dot{e} \end{aligned} \tag{32}$$

Combining (5), (11) and (26), the close loop system equation can be derived as

$$M(q)(\ddot{e} + K_p(e)e + K_d(e)\dot{e}) - \Delta\xi_{dis} - v = 0 \tag{33}$$

Since $M(q) = M^T(q) > 0$, thus (33) can be rewritten as

$$\ddot{e} = -K_p(e)e - K_d(e)\dot{e} + M^{-1}(q)(\Delta\xi_{dis} + v) \tag{34}$$

Substituting (34) into (32), (32) can be rewritten as

$$\begin{aligned} \dot{L}(e, \dot{e}) &= \dot{e}^T \ddot{e} + e^T K_p(e) \dot{e} \\ &= -\dot{e}^T K_d(e) \dot{e} + \dot{e}^T M^{-1}(q)(\Delta\xi_{dis} + v) \end{aligned} \tag{35}$$

Because

$$\begin{aligned} &\dot{e}^T M^{-1}(q)(\Delta\xi_{dis} + v) \\ &= \dot{e}^T M^{-1}(q)\Delta\xi_{dis} + \dot{e}^T M^{-1}(q) v \\ &= \dot{e}^T M^{-1}(q)\Delta\xi_{dis} - \left\|\dot{e}^T M^{-1}(q)\right\| b_d \\ &\leq 0 \end{aligned} \tag{36}$$

and $K_d(e)$ is a positive definite matrix, the below result can be obtained as

$$\dot{L}(e, \dot{e}) \leq -\dot{e}^T K_d(e) \dot{e} \leq 0 \tag{37}$$

Therefore, according to the Lyapunov stability theory, the closed loop system is stable. In the region:

$$\Phi = \left\{ \begin{bmatrix} e \\ \dot{e} \end{bmatrix} : \dot{L}(e, \dot{e}) = 0 \right\} = \left\{ \begin{bmatrix} e \\ \dot{e} \end{bmatrix} = \begin{bmatrix} e \\ 0 \end{bmatrix} \in \Re^4 \right\}$$

$\begin{bmatrix} e & \dot{e} \end{bmatrix}^T = 0$ is the unique invariant set. Based on the LaSalle's invariance theorem, the closed loop system is asymptotically stable.

V. SIMULATION AND EXPERIMENT RESULTS

A. SIMULATION RESULTS

In this section, the co-simulations are employed to validate the effectiveness and robustness of the proposed controller in application of the designed SMM. Since the inverse dynamics decoupling term is used in the control system, the controller parameters can be tuned independently in the α and β directions. Simultaneously, the simulation model of FPDESO controller is established to generate control signals for the dynamic simulation model established by ADAMS, as illustrated in Fig. 11. The relevant structure parameters employed in the simulations are listed in Table 2.

To demonstrate the effectiveness of the proposed controller, the following four different control schemes are simulated.

1) FPDESO: This is the FPD inverse dynamics decoupling control scheme (26) with FLESO (21) proposed in this paper. The relevant parameters are set as follows:

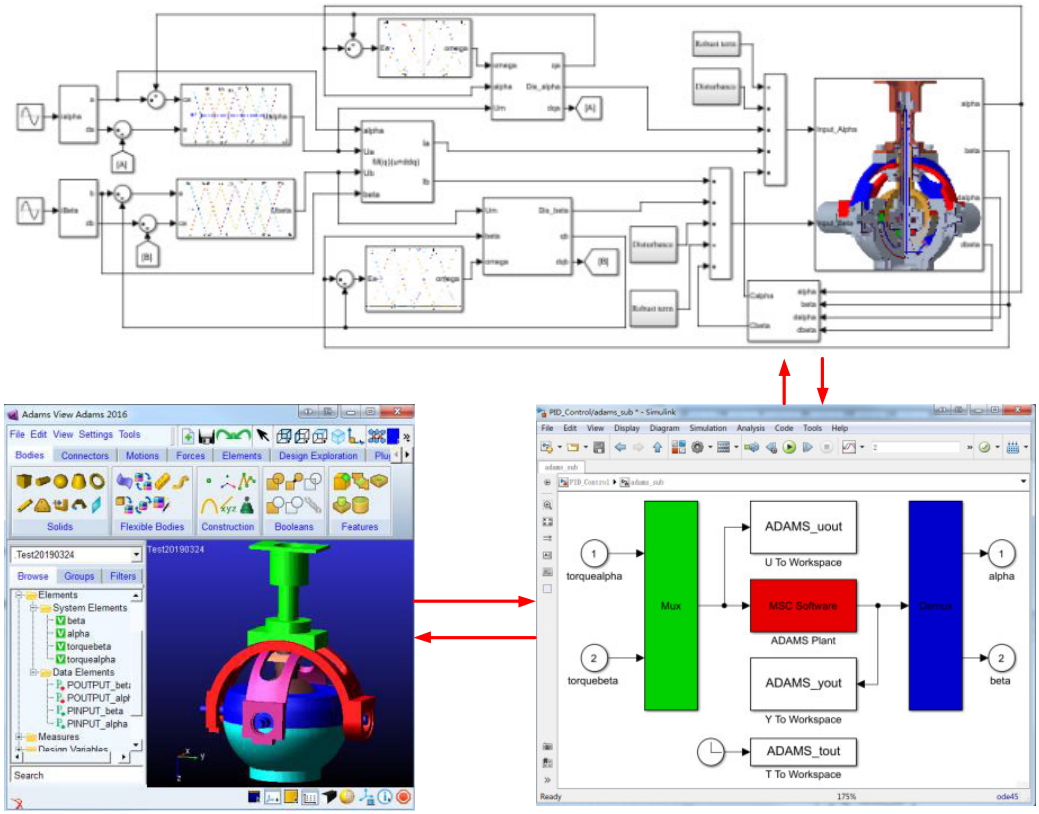

FIGURE 11. Co-simulation models.

TABLE 2. Structure parameters of the SMM.

Part	Symbol	Quantity	Value
Rudder blade	m_b	Mass	3.9 (kg)
	l_b	Length	5.0 (mm)
	I_b	Moment of inertia	[0.027 0.027 0.005](kg.m^2)
Spin motor	m_m	Mass	1.2 (kg)
	l_m	Length	3.5 (mm)
	I_m	Moment of inertia	[0.01 0.01 0.01] (kg.m^2)
Rotor	m_r	Mass	5.4 (kg)
	l_r	Length	3.0 (mm)
	I_r	Moment of inertia	[0.032 0.032 0.056](kg.m^2)

The control gains are given as $k_e = diag(2, 6)$, $k_{de} = diag(5, 2)$, $k_1 = diag(10, 13)$, and $k_2 = diag(0.5, 0.9)$. The initial values is selected as $k_{pj_0} = diag(4050, 4150)$ and $k_{dj_0} = diag(110, 90)$. The gains are given as $k_{s1} = diag(3, 5)$, $k_{s2} = diag(1.15, 0.98)$ and $k_w = diag(11, 20)$. The initial value of the bandwidth is given as $\omega_0 = diag(20, 28)$.The gain of robust term is set as $b_d = diag(0.03\pi, 0.02\pi)$.

2) PID: This is a proportional-integral-derivative controller. The controller gains tuned carefully via trial and error method are $k_p' = diag(10, 50)$, $k_i' = diag(0.9, 3)$ and $k_d' = diag(1.5, 0.5)$, which represent the P-, I- and D-gains, respectively. Set the filter coefficient as $f' = diag(500, 1456)$.

3) NPD: This is a nonlinear proportional-derivative controller [37] defined in (38). Compared with the PID, NPD can provide better control performance. Nonetheless, the structure of NPD becomes complicated and parameters that need to be tuned also increase.

$$u_{NPD} = K_{Np}(e(t))e(t) + K_{Nd}(\dot{e}(t))\dot{e}(t) \tag{38}$$

with

$$K_{Np}(e(t)) = \begin{cases} k_{Npj}\,|e(t)|^{\rho_{pj}-1}, & |e(t)| > \delta_{pj} \\ k_{Npj}\delta_{pj}^{\rho_{pj}-1}, & |e(t)| \le \delta_{pj} \end{cases} \quad j = \alpha, \beta \tag{39}$$

$$K_{Nd}(\dot{e}(t)) = \begin{cases} k_{Ndj}\,|\dot{e}(t)|^{\rho_{dj}-1}, & |\dot{e}(t)| > \delta_{dj} \\ k_{Ndj}\delta_{dj}^{\rho_{dj}-1}, & |\dot{e}(t)| \le \delta_{dj} \end{cases} \quad j = \alpha, \beta \tag{40}$$

where $K_{Np}(e(t))$ and $K_{Nd}(\dot{e}(t))$ are the time-varying nonlinear proportional and derivative gains, respectively, $\rho_{\cdot j}$ determines the nonlinearity of the controller, when $\rho_{\cdot j} = 1$, the controller degrades into the linearity, $\delta_{\cdot j}$is the threshold value of error or change of error.

The initial values of P- and D-gains can be given as $K_{Np} = diag(29, 20)$ and $K_{Nd} = diag(0.8, 0.5)$. The threshold values are selected as $\sigma_p = diag(0.1, 0.1)$ and $\sigma_d = diag(0.1, 0.2)$. The nonlinearity coefficients are chosen as $\rho_p = diag(1.2, 0.6)$ and $\rho_d = diag(1.1, 0.8)$.

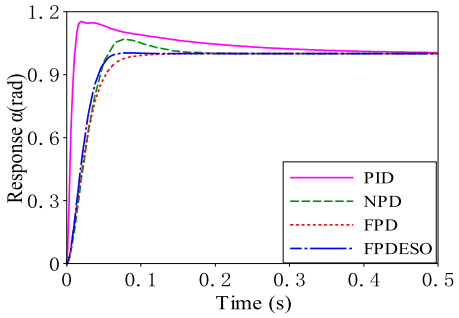

FIGURE 12. Step response of four controllers in the α direction.

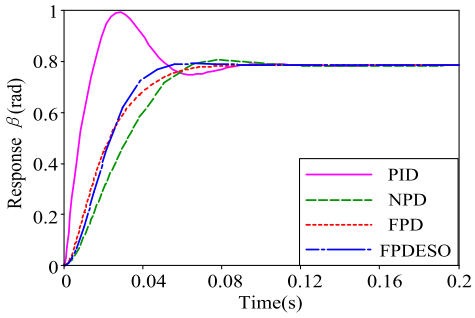

FIGURE 13. Step response of four controllers in the β direction.

4) FPD: This is a controller combining the fuzzy logic system with the proportional-derivative controller. The control gains are given as $k'_e = diag(8, 5), k'_{de} = diag(2, 3)$, $k'_1 = diag(1.5, 5)$, and $k'_2 = diag(0.5, 0.8)$. The initial values of P- and D-gains are set as $k_{fp} = diag(41, 45)$ and $k_{fd} = diag(1.1, 0.9)$, respectively.

To evaluate the proposed controller comprehensively, two cases are investigated.

Case 1: Trajectory tracking in the absence of disturbances

In this case, it is assumed that the SMM is operated under the ideal condition without the modeling errors and external disturbances. The initial position and velocity vectors are both set to be zero. First, study the response characteristics of four controllers under the step signal input.

According to the step response curves, as depicted in Figs. 12 and 13, among four controllers, PID achieves the fastest response (0.01 s and 0.01 s) and the largest overshoot (0.153 rad and 0.195 rad) in the α and β directions, respectively. On the premise of maintaining a certain response speed (0.08 s and 0.07 s), NPD can suppress overshoot to a certain extent but not completely eliminate it (0.075 rad and 0.022 rad). And FPD can effectively restrain the oscillations and overshoot (0 rad and 0 rad), but it also reduces the response speed (0.14 s and 0.09 s). It is worth noting that the proposed FPDESO controller has a trade-off between response speed and overshoot in both the α and β directions respectively with a rise time of 0.06 s and 0.05 s, and almost no overshoot.

Without loss of generality, the smooth sinusoid (41) is selected as the reference trajectory for simulation to further verify the tracking performance of the proposed controller. The maximal angular velocities in the α and β directions are π rad/s and 0.785π rad/s, respectively, which can effectively assess the tracking ability of the proposed controller.

$$q = [s(\pi t) \quad 0.785s(\pi t)]^T \tag{41}$$

The tracking trajectories and tracking errors in the α and β directions under four controllers are shown in Figs. 14-17, respectively.

As shown in Figs. 15 and 17, it can be observed that the PID controller gives a large tracking error about 0.012 rad and 0.003 rad in the α and β directions respectively, and

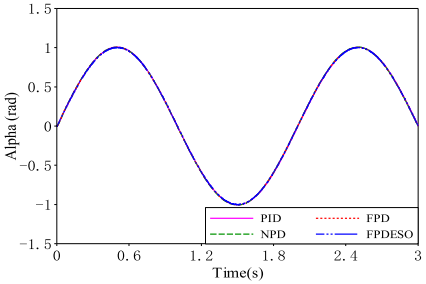

FIGURE 14. Tracking trajectory in the α direction.

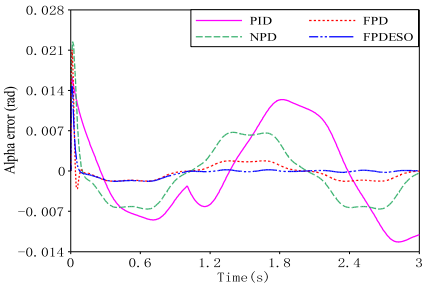

FIGURE 15. Tracking error in the α direction.

has an obvious oscillation. The NPD controller provides an improved tracking performance with the maximal absolute errors being about 0.007 rad and 0.003 rad in the α and β directions respectively. Since the FPDESO controller decouples the coupling system and thus achieves the independent adjustment of controller parameters in the α and β directions, it can provide the excellent tracking performance. Furthermore, the response trajectories under the FPDESO controller can quickly track the desired trajectories and maintain a small error, while the other three controllers always have large errors in the whole tracking process.

The following four performance indices will be employed to further evaluate the quality of control algorithms, i.e., the maximal absolute tracking error, average tracking error, root mean square tracking error (RMS) and control energy, defined as follows:

1) M_a is the maximal absolute tracking error as a transient index denoting the ultimate performance, which is defined as

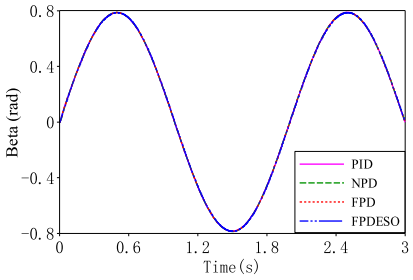

FIGURE 16. Tracking trajectory in the β direction.

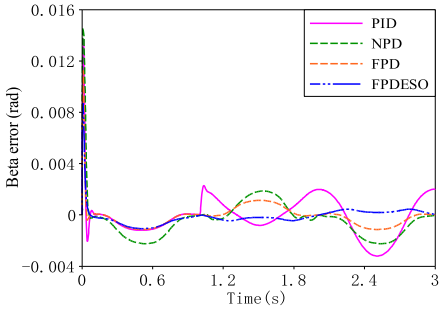

FIGURE 17. Tracking error in the β direction.

$$M_a = \max\{|e|\} \tag{42}$$

2) A_{ve} is the average tracking error, which is defined as

$$A_{ve} = \frac{1}{n}\sum_{i=1}^{n}|e(i)| \tag{43}$$

3) R_{MS} is the root mean square tracking error representing the average performance in the entire operating cycle, which is defined as

$$R_{MS} = \sqrt{\frac{1}{t_f}\int_0^{t_f} e^2 dt} \tag{44}$$

4) ε_u is the control energy denoting the control intensity of the controller, which is defined as

$$\varepsilon_u = \int_0^{t_f} u^2(t)dt \tag{45}$$

where t_f is the final time.

The performance indices of four controllers are listed in Table. 3. As shown, compared with the other three controllers, the RMS values under the proposed controller are the smallest in two directions about 0.0022 rad and 0.0012 rad respectively, which are 29% and 29.4% lower than those of the FPD controller. The maximal absolute and average tracking errors are both lower than the other three controllers as well. Meanwhile, it requires the least control energy about 24.44 J and 2.126 J, which indicates the proposed controller outperforms the other three controllers in terms of the trajectory tracking precision and control energy.

Case 2: Robustness testing against disturbances

TABLE 3. Performance indices of the α and β directions in case 1.

Indices	M_a	A_{ve}	R_{MS}	ε_u
PID	0.012/0.003	0.0070/0.001	0.0079/0.0017	65.87/22.05
NPD	0.007/0.003	0.0045/0.001	0.0056/0.0021	48.22/13.03
FPD	0.001/0.002	0.0008/0.0007	0.0031/0.0017	33.71/11.28
FPDESO	0.0008/0.0008	0.0004/0.0003	0.0022/0.0012	24.44/2.216

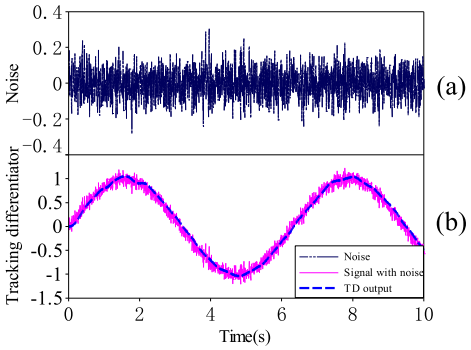

FIGURE 18. TD performance.

To further verify the tracking performance and robustness of the proposed controller, the operating condition with disturbances and noise is simulated. In this simulation stage, sensor noise as shown in Fig. 20(a) and disturbances defined in (46) are considered.

$$\tau_d = \begin{cases} [0 \;\; 0] & t \le 1 \\ [-0.5c(7t) \;\; 0.5c(7t)] & t > 1 \end{cases} \tag{46}$$

From the results in *Case 1*, comparatively speaking, the PID and NPD controllers have the worst performance, so they are omitted in this case. Meanwhile, to ensure comparability, the parameters of the FPD and FPDESO controllers are set to be consistent with *Case 1*.

To reduce the influence of sensor noise, TD defined in (25) is utilized to extract the actual signal from measuring signal by virtue of eliminating noise. The filtering performance of the TD is shown in Fig. 18(b).

The tracking trajectories of two controllers are shown in Figs. 19 and 20. The maximal absolute tracking errors under the FPD controller are 0.127 rad and 0.131 rad in the α and β directions, respectively. Nevertheless, since the FPDESO controller utilizes the FLESO to estimate and compensate for the total disturbances, it is capable to suppress these unexpected disturbances effectively. It can be seen that the response trajectories under the FPDESO controller track the desired trajectories well, and the maximal absolute tracking errors in two directions are about 0.099 rad and 0.095 rad, respectively. Since the tracking performance can be illustrated clearly by the tracking trajectory, the tracking error curve is omitted in this case.

The performance indices of two controllers in the presence of disturbances are listed in Table 4. As can be seen from the results, the performance indices of the FPDESO controller are all better than those of the FPD controller. The RMS values

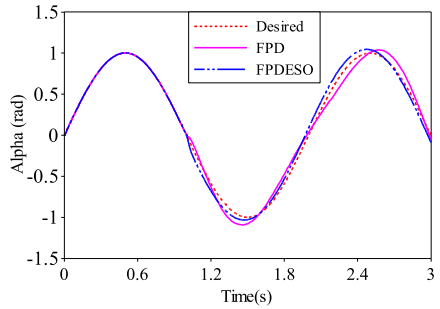

FIGURE 19. Tracking trajectory in the α direction.

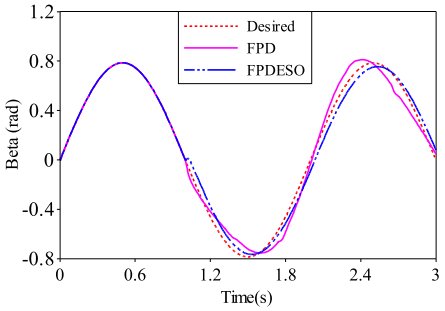

FIGURE 20. Tracking trajectory in the β direction.

(0.0120 rad and 0.0105 rad) under the FPDESO controller are much smaller than those of FPD (0.0274 rad and 0.0168 rad), with almost 56% and 38% performance improvement in the α and β directions, respectively.

Obviously, due to the model uncertainties and external disturbances, the tracking performance of the FPD controller is seriously degraded. In contrary, since the FLESO is utilized to estimate and compensate for the model uncertainties and external disturbances, the tracking performance under the FPDESO controller will not be affected evidently. Therefore, the disturbances rejection capability and robustness of the proposed controller are validated.

B. EXPERIMENT RESULTS

To further evaluate the effectiveness of the proposed control strategy, experiments are accomplished on a prototype SMM. The schematic of the hydraulic system used in the test bench shown in Fig. 21 is composed of a hydraulic power unit, two servo valves, a control module, two encoders and an SMM.

The real-time control system consists of a digital signal processor (DSP), A/D card, D/A card, V/I converter and host computer, as depicted in Fig. 22. Utilize the Labview2018 to program a graphical user interface on the host computer, which can be used to accomplish operating modes choice, data storage and results display. The relevant hardware specifications of the control system are listed in Table. 5.

According to the simulation results, two controllers with outstanding tracking performance, FPD and FPDESO, are utilized for experiments to verify the effectiveness of the

TABLE 4. Performance indices of the α and β directions in case 2.

Indices	FPD	FPDESO
M_a	0.127/0.131	0.099/0.095
A_{ve}	0.0564/0.0513	0.044/0.040
R_{MS}	0.0274/0.0168	0.0120/0.0105
$\mathcal{E}_u$	43.44/24.67	38.63/11.01

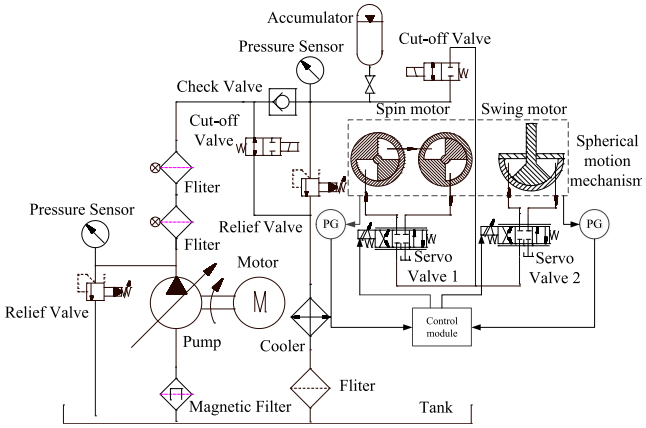

FIGURE 21. Schematic of the hydraulic system.

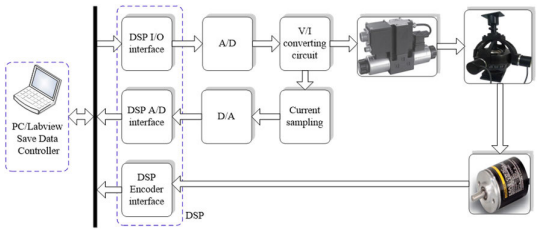

FIGURE 22. Schematic diagram of the real-time control system.

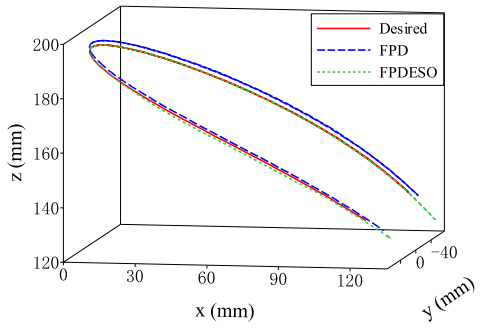

FIGURE 23. Experiment results under FPD and FPDESO.

proposed control strategy. Since the position of the end-effector of the SMM, $(x, y, z)^T = L(s\beta s\theta, -s\beta c\theta, c\beta)^T$, is more concerned in the practical application, it is investigated.

The tracking trajectories and absolute position errors of the end-effector under the FPD and FPDESO controllers are shown in Figs. 23-25, respectively. It is observed that the tracking trajectory under the proposed FPDESO controller has a small fluctuation within an acceptable range,

TABLE 5. Hardware specifications of the control system.

Component	Item		Value
DSP	Type		TMS320C6657
	Clock frequency		1.25GHz
A/D, D/A	Type		MAX1309/AD5754R
	Channels		4/4
	Resolution		12bits/16bits
V/I	Type		OPA549
	Range		±30 V
Servo valve	Nominal flow with Δp 10 bar P-T (L/min)		26
	Reference time±100%	Rising response time (ms)	50
		Fall response time (ms)	25
Encoder	Maximum response Frequency (kHz)		200
	Slewing speed (r/min)		12000

TABLE 6. Performance indices in the x, y and z directions.

Indices	M_a	A_{ve}	R_{MS}
FPD	1.518/2.022/1.913	0.710/0.678/0.762	0.852/0.856/0.942
FPDESO	0.924/1.078/1.071	0.371/0.594/0.504	0.446/0.683/0.584

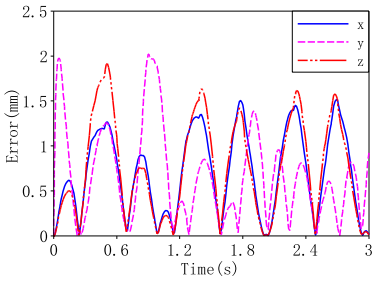

FIGURE 24. Position absolute errors under FPD.

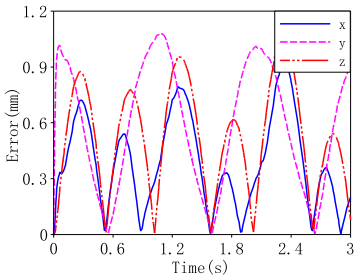

FIGURE 25. Position absolute errors under FPDESO.

and the maximal absolute tracking errors in the x, y and z directions are approximately 0.924 mm, 1.078 mm and 1.071 mm, respectively. Nevertheless, the maximal absolute tracking errors under the FPD controller in the x, y and z directions are 1.518 mm, 2.022 mm and 1.913 mm respectively, which are significantly larger than those of FPDESO. Meanwhile, the RMS values under the FPD controller, as shown in Table 6, are about 47.7%, 20.2% and 38% higher than those of the proposed control law in the x, y and z directions,

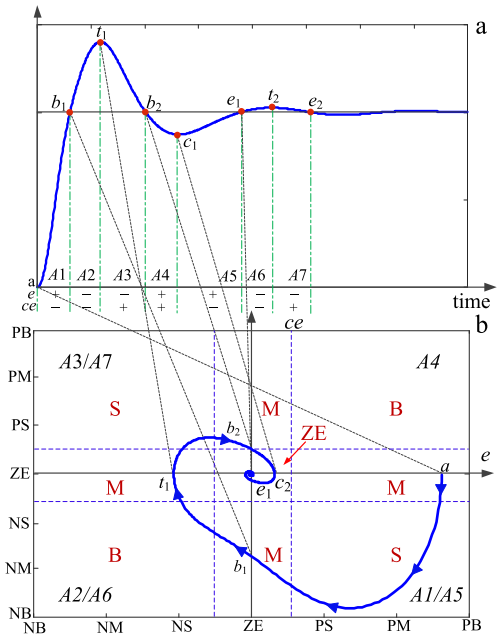

FIGURE 26. Rule analysis for β a) Step response b) (e, ce) state space.

respectively. Therefore, the experimental results show that compared with the FPD controller, the proposed FPDESO controller can provide much better tracking performance, which verifies the effectiveness of the proposed controller.

VI. CONCLUSION

A novel hybrid control scheme, which consists of a fuzzy PD control with varying gains, inverse dynamic model-based feed-forward decoupling term, FLESO with varying bandwidth and robust term, is proposed for the trajectory tracking control of the SMM considering the influence of model uncertainties and external disturbances. The asymptotic stability of the mentioned controller was proved by the Lyapunov direct method. A comprehensive comparison was implemented with other three controllers named PID, NPD and FPD. Compared with FPD, the proposed FPDESO controller can reduce the RMS values in the x, y and z directions by about 47.7%, 20.2% and 38%, respectively. The simulation results verified that the proposed controller can effectively handle the model uncertainties and external disturbances. The experimental results also validated the feasibility of the proposed controller.

This paper provided an alternative scheme with the simple structure and satisfactory control performance for the system in the presence of multi-variable nonlinearity, uncertainties and strong coupling.

APPENDIX A

The explicit expressions of the relevant terms in (2) except the viscous friction and external disturbances are given as follows:

$$M(q) = \begin{bmatrix} M_{11} & M_{12} \\ M_{21} & M_{22} \end{bmatrix}, \quad C(q, \dot{q}) = \begin{bmatrix} C_{11} & C_{12} \\ C_{21} & C_{22} \end{bmatrix},$$

TABLE 7. Rules for f_k^{β} (k_e) and f_k^{β} (k_{de}).

ce \ e	NB	NM	NS	ZE	PS	PM	PB
NB	PB\PB	PB\PB	PB\PB	NM\NM	PS\PS	PS\PS	ZE\ZE
NM	PB\PB	PB\PB	PB\PB	NS\NM	PS\PS	ZE\ZE	PS\PS
NS	PB\PM	PB\PM	PM\PM	NS\NM	ZE\ZE	PS\PS	PM\PS
ZE	NM\ZE	NM\NS	NM\NS	ZE\ZE	PM\NS	PM\NS	PM\ZE
PS	NM\NS	NS\NS	ZE\ZE	PS\PM	NM\NS	NM\NS	NM\NS
PM	NS\NS	ZE\ZE	NS\NS	PS\PM	NM\NB	NB\NB	NB\NB
PB	ZE\ZE	NS\NS	NM\NM	PM\PM	NB\NB	NB\NB	NB\NB

$$
\begin{aligned}
G(q) &= \begin{bmatrix} G_{11} \\ G_{21} \end{bmatrix} \\
M_{11} &= I_{44} + \sec^2\alpha c^2\beta \left(\tan^2\alpha + c^2\beta\right)^{-2} \\
&\quad \begin{bmatrix} I_{55}\sec^2\alpha \\ -I_{11}\left(\tan^2\alpha + c^2\beta\right) \end{bmatrix} \\
M_{12} &= M_{21} = \tan\alpha s\beta c\beta \left(\tan^2\alpha + c^2\beta\right)^{-2} \\
&\quad \begin{bmatrix} I_{55}\sec^2\alpha \\ -0.5I_{11}\left(\tan^2\alpha + c^2\beta\right) \end{bmatrix} \\
M_{22} &= I_{22} + I_{55}\tan^2\alpha s^2\beta \left(\tan^2\alpha + c^2\beta\right)^{-2} \\
C_{11} &= \sec^5\alpha c\beta \left(\tan^2\alpha + c^2\beta\right)^{-3} \\
&\quad \begin{bmatrix} 2s\alpha c\beta\left(I_{11}c^2\alpha s^2\beta - I_{55}\tan^2\alpha\right)\dot{\alpha} \\ +c\alpha s\beta\left(2I_{11}s^2\alpha - I_{55}\tan^2\alpha + I_{55}c^2\beta\right)\dot{\beta} \end{bmatrix} \\
C_{12} &= \sec^2\alpha \left(\tan^2\alpha + c^2\beta\right)^{-3} \\
&\quad \begin{bmatrix} s\beta c\beta\left(2I_{55}\tan^2\alpha - 0.5I_{11}c^2\beta\right)\dot{\alpha} \\ +\tan\alpha c^2\beta\left(I_{55}\sec^2\alpha - 0.5I_{11}\right)\dot{\beta} \end{bmatrix} \\
C_{21} &= \sec^2\alpha \left(\tan^2\alpha + c^2\beta\right)^{-3} \\
&\quad \begin{bmatrix} s\beta c\beta\left(I_{55}\sec^4\alpha + 0.5I_{11}\tan^2\alpha\right)\dot{\alpha} \\ -\tan\alpha s^2\beta\left(I_{55}\sec^2\alpha - 0.5I_{11}s^2\alpha\right)\dot{\beta} \end{bmatrix} \\
C_{22} &= I_{55}\sec^2\alpha \left(\tan^2\alpha + c^2\beta\right)^{-3} \\
&\quad \begin{bmatrix} \tan\alpha s^2\beta\left(c^2\beta - \tan^2\alpha\right)\dot{\alpha} \\ +s^2\alpha s\beta c\beta\left(\sec^2\alpha + s^2\beta\right)\dot{\beta} \end{bmatrix} \\
G_{11} &= 0 \\
G_{12} &= -\left(m_b g l_{b0} + m_r g l_{r0} + m_m g l_{m0}\right) s\beta \\
I_{11} &= I_{m.zz} + 2I_{r.zz}, I_{22} = I_{d.xx} + I_{m.xx} + I_{r.xx}, \\
I_{33} &= I_{d.zz} + I_{m.zz} + I_{r.zz} \\
I_{44} &= I_{m.zz}/4 + I_{r.zz}, I_{55} = (I_{22} + I_{33})/2
\end{aligned}
$$

APPENDIX B

The step response and corresponding phase plane trajectory in the β direction are shown in Fig. 26(a) and (b), respectively. See Table 7.

REFERENCES

[1] H. Asada and J. Granito, "Kinematic and static characterization of wrist joints and their optimal design," in *Proc. IEEE Int. Conf. Robot. Autom.*, St. Louis, MO, USA, May 1985, pp. 244–250.

[2] Y. X. Su, B. Y. Duan, B. Peng, and R. D. Nan, "Singularity analysis of fine-tuning stewart platform for large radio telescope using genetic algorithm," *Mechatronics*, vol. 13, no. 5, pp. 413–425, Jun. 2003.

[3] M. Ruggiu, "Kinematic and dynamic analysis of a two-degree-of-freedom spherical wrist," *J. Mech. Robot.*, vol. 2, no. 3, pp. 191–220, Aug. 2010.

[4] B. Bian and L. Wang, "Design, analysis, and test of a novel 2-DOF spherical motion mechanism," *IEEE Access*, vol. 8, pp. 53561–53574, 2020.

[5] H.-X. Li, L. Zhang, K.-Y. Cai, and G. Chen, "An improved robust fuzzy-PID controller with optimal fuzzy reasoning," *IEEE Trans. Syst., Man, Cybern. B, Cybern.*, vol. 35, no. 6, pp. 1283–1294, Dec. 2005.

[6] P. S. Londhe, Y. Singh, M. Santhakumar, B. M. Patre, and L. M. Waghmare, "Robust nonlinear PID-like fuzzy logic control of a planar parallel (2PRP-PPR) manipulator," *ISA Trans.*, vol. 63, pp. 218–232, Jul. 2016.

[7] W. He, Y. Chen, and Z. Yin, "Adaptive neural network control of an uncertain robot with full-state constraints," *IEEE Trans. Cybern.*, vol. 46, no. 3, pp. 620–629, Mar. 2016.

[8] S. S. Ge, C. C. Hang, and L. C. Woon, "Adaptive neural network control of robot manipulators in task space," *IEEE Trans. Ind. Electron.*, vol. 44, no. 6, pp. 746–752, Dec. 1997.

[9] L. Zhao, H. Cheng, and T. Wang, "Sliding mode control for a two-joint coupling nonlinear system based on extended state observer," *ISA Trans.*, vol. 73, pp. 130–140, Feb. 2018.

[10] L. A. Zadeh, "Outline of a new approach to the analysis of complex systems and decision processes," *IEEE Trans. Syst., Man, Cybern.*, vol. SMC-3, no. 1, pp. 28–44, Jan. 1973.

[11] H. Mamdani and S. Assilian, "Applications of fuzzy algorithms for control of simple dynamic plant," *Inst. Elect. Eng.*, vol. 121, no. 12, pp. 1585–1588, 1974.

[12] G. Feng, "A survey on analysis and design of model-based fuzzy control systems," *IEEE Trans. Fuzzy Syst.*, vol. 14, no. 5, pp. 676–697, Oct. 2006.

[13] Y. Singh and M. Santhakumar, "Inverse dynamics and robust sliding mode control of a planar parallel (2-PRP and 1-PPR) robot augmented with a nonlinear disturbance observer," *Mechanism Mach. Theory*, vol. 92, pp. 29–50, Oct. 2015.

[14] R. K. Mudi and N. R. Pal, "A self-tuning fuzzy PI controller," *Fuzzy Sets Syst.*, vol. 115, no. 2, pp. 327–338, Oct. 2000.

[15] C. Liu, J.-F. Peng, F.-Y. Zhao, and C. Li, "Design and optimization of fuzzy-PID controller for the nuclear reactor power control," *Nucl. Eng. Des.*, vol. 239, no. 11, pp. 2311–2316, 2009.

[16] X. Jin, K. Chen, Y. Zhao, J. Ji, and P. Jing, "Simulation of hydraulic transplanting robot control system based on fuzzy PID controller," *Measurement*, vol. 164, pp. 108023–108029, Nov. 2020.

[17] D. Pan, F. Gao, Y. Miao, and R. Cao, "Co-simulation research of a novel exoskeleton-human robot system on humanoid gaits with fuzzy-PID/PID algorithms," *Adv. Eng. Softw.*, vol. 79, pp. 36–46, Jan. 2015.

[18] G. J. Liu and A. A. Goldenberg, "Experiments on robust control of robot manipulators," in *Proc. IEEE Int. Conf. Robot. Autom.*, Nice, France, May 1992, pp. 1935–1940.

[19] T. D. Le, H.-J. Kang, Y.-S. Suh, and Y.-S. Ro, "An online self-gain tuning method using neural networks for nonlinear PD computed torque controller of a 2-dof parallel manipulator," *Neurocomputing*, vol. 116, pp. 53–61, Sep. 2013.

[20] Q.-C. Zhong and D. Rees, "Control of uncertain LTI systems based on an uncertainty and disturbance estimator," *J. Dyn. Syst., Meas., Control*, vol. 126, no. 4, pp. 905–910, Dec. 2004.

[21] S.-C. Lee and H.-S. Ahn, "Robot manipulator adaptive control using disturbance estimator," in *Proc. Int. Conf. Control, Autom. Inf. Sci. (ICCAIS)*, Dec. 2014, pp. 41–46.

[22] W.-H. Chen, D. J. Ballance, P. J. Gawthrop, and J. O'Reilly, "A nonlinear disturbance observer for robotic manipulators," *IEEE Trans. Ind. Electron.*, vol. 47, no. 4, pp. 932–938, Aug. 2000.

[23] T. Ren, Y. Dong, D. Wu, and K. Chen, "Collision detection and identification for robot manipulators based on extended state observer," *Control Eng. Pract.*, vol. 79, pp. 144–153, Oct. 2018.

[24] S. E. Talole, J. P. Kolhe, and S. B. Phadke, "Extended-state-observer-based control of flexible-joint system with experimental validation," *IEEE Trans. Ind. Electron.*, vol. 57, no. 4, pp. 1411–1419, Apr. 2010.

[25] A. A. Godbole, J. P. Kolhe, and S. E. Talole, "Performance analysis of generalized extended state observer in tackling sinusoidal disturbances," *IEEE Trans. Control Syst. Technol.*, vol. 21, no. 6, pp. 2212–2223, Nov. 2013.

[26] K. M. Passino and S. Yurkovich, *Fuzzy Control*. Menlo Park, CA, USA: Addison-Wesley, 1998.

[27] S. Boverie, B. Demaya, and A. Titli, "Fuzzy logic control compared with other automatic control approaches," in *Proc. 30th IEEE Conf. Decis. Control*, Brighton, U.K., Dec. 1991, pp. 1212–1216.
[28] H.-X. Li and H. B. Gatland, "A new methodology for designing a fuzzy logic controller," *IEEE Trans. Syst., Man, Cybern.*, vol. 25, no. 3, pp. 505–512, Mar. 1995.
[29] C. C. Lee, "Fuzzy logic in control systems: Fuzzy logic controller," *IEEE Trans. Syst. Man, Cybern.*, vol. 20, no. 2, pp. 404–435, Apr. 1990.
[30] Q. Zheng, Z. Chen, and Z. Gao, "A practical approach to disturbance decoupling control," *Control Eng. Pract.*, vol. 17, no. 9, pp. 1016–1025, Sep. 2009.
[31] Z. Gao, "Scaling and bandwidth-parameterization based controller tuning," in *Proc. Amer. Control Conf.*, Denver, CO, USA, Jun. 2003, pp. 4989–4996.
[32] R. Madoński and P. Herman, "Survey on methods of increasing the efficiency of extended state disturbance observers," *ISA Trans.*, vol. 56, pp. 18–27, May 2015.
[33] Q. Chen, N. Yu-Rong, Z. Heng-Huo, and R. Xue-Mei, "Full-order sliding mode control of uncertain chaos in a permanent magnet synchronous motor based on a fuzzy extended state observer," *Chin. Phys. B*, vol. 24, no. 11, pp. 1105411–1105416, 2015.
[34] M. Naghdi and M. A. Sadrnia, "A novel fuzzy extended state observer," *ISA Trans.*, vol. 102, pp. 1–11, Jul. 2020.
[35] C. Du, Z. Yin, Y. Zhang, J. Liu, X. Sun, and Y. Zhong, "Research on active disturbance rejection control with parameter autotune mechanism for induction motors based on adaptive particle swarm optimization algorithm with dynamic inertia weight," *IEEE Trans. Power Electron.*, vol. 34, no. 3, pp. 2841–2855, Mar. 2019.
[36] M. A. Llama, R. Kelly, and V. Santibanez, "Stable computed-torque control of robot manipulators via fuzzy self-tuning," *IEEE Trans. Syst., Man, Cybern. B, Cybern.*, vol. 30, no. 1, pp. 143–150, Feb. 2000.
[37] J. Q. Han, "Nonlinear PID controller," *Acta Automatica Sinica*, vol. 20, no. 4, pp. 487–490, Apr. 1994.

BIN BIAN received the master's degree from Yanshan University, China, in 2013. He is currently pursuing the Ph.D. degree in mechanical engineering with Beihang University, Beijing, China. His research interests include robotic structure and control and hydraulic power transmission and control.

LIANG WANG received the B.S. degree from the Harbin Shipbuilding Engineering Institute, in 1985, the M.S. degree from the Harbin Institute of Technology, in 1988, and the Ph.D. degree from Beihang University, in 2000. He is currently a Professor and a Supervisor for Ph.D. student with Beihang University. His main research interests include robotic structure and control, human-machine systems, mechatronics, and hydraulic power transmission and control.